LITERATURE CITED

Angus, J. C., et al., "Thermogravimetric Measurements At High Pressures Using a Hanging Reactor Thermobalance," Annual Meeting of AIChE, Paper No. 12b, Chicago (Nov. 16–20, 1980).

Aris, R., *Elementary Chemical Reactor Analysis*, Prentice-Hall, Englewood Cliffs, NJ (1969).

Badzioch, S., D. R. Gregory, and M. A. Field, "Investigation of the Temperature Variation of the Thermal Conductivity and Thermal Diffusivity of Coal," *Fuel*, **43**, 267 (1964).

Bischoff, K. B., "Accuracy of the Pseudo Steady State Approximation for Moving Boundary Diffusion Problems," *Chem. Eng. Sci.*, **18**, 711 (1963).

Blackwood, J. D., and A. J. Ingeme, "The Reaction of Carbon with Carbon Dioxide at High Pressure," *Aust. J. Chem.*, **13**, 194 (1960).

Dutta, S., C. Y. Wen, and R. J. Belt, "Reactivity of Coal and Char. 1. In Carbon Dioxide Atmosphere," *Ind. Eng. Chem. Process Des. Dev.*, **16**, No. 1, 20 (1977).

Feldkirchner, H. L., and J. Huebler, "Reaction of Coal with Steam-Hydrogen Mixtures at High Temperatures and Pressures," *Ind. Eng. Chem. Process Des. Dev.*, **4**, 134 (1965).

Gan, H., S. P. Nandi, and P. L. Walker, Jr., "Nature of the Porosity in American Coals," *Fuel*, **51**, 272 (1972).

Gardner, N. C., J. J. Leto, S. Lee, and J. C. Angus, "Thermogravimetric Measurements at High Pressures," *NBS Special Publication*, **580**, 235 (1980).

Ishida, M., and C. Y. Wen, "Comparison of Kinetic and Diffusional Models for Solid-Gas Reactions," *AIChE J.*, **14**, No. 2, 311 (1968).

Laurendeau, N. M., "Heterogeneous Kinetics of Coal Char Gasification and Combustion," *Prog. Energy Combust. Sci.*, **4**, 221 (1978).

Lee, S., "Coal Char Gasification Studies," Ph.D. Dissertation, Case Western Reserve University (1980).

Mahajan, O. P., R. Yarzab, and P. L. Walker, Jr., "Unification of Coal-Char Gasification Reaction Mechanisms," *Fuel*, **57**, 643 (1978).

Marsh, H., "The Determination of Surface Areas of Coals—Some Physicochemical Considerations," *Fuel*, **44**, 253 (1965).

Petersen, E. E., "Chemical Reaction Analysis," Prentice-Hall, Englewood Cliffs, NJ (1965).

Walker, Jr., P. L., F. Rusinko, Jr., and L. G. Austin, *Advances in Catalysis*, **XI**, 133, Academic Press, New York (1959).

Wicke, E., "Contributions to the Combustion Mechanism of Carbon," Fifth Symp. on Combustion, 245, Reinhold, New York (1955).

Manuscript received January 20, 1983; revision received May 26, and accepted July 1, 1983.

Liquid-Phase Diffusion and Adsorption of Pyridine in Porous Silica-Alumina Pellets

The adsorption and effective diffusivity of pyridine dissolved in heptane were measured in silica-alumina pellets using a specially developed single-pellet continuous-flow diffusion cell. The measured diffusivities varied between 0.43×10^{-9} and 3.25×10^{-9} $m^2 \cdot s^{-1}$; the temperature dependence of the diffusivities indicated that both pore volume diffusion and surface diffusion play a role in the mass transfer.

D. S. van VUUREN

Chemical Engineering Research Group—CSIR
Pretoria, Republic of South Africa

C. M. STANDER

National Physical Research Laboratory—CSIR
Pretoria, Republic of South Africa

DAVID GLASSER

Dept. of Chemical Engineering
University of the Witwatersrand
Johannesburg, Republic of South Africa

SCOPE

The heterocyclic nitrogen compounds present in fossil-fuel liquids like shale oils, petroleum and coal liquids cause problems such as catalyst poisoning during processing and formation of excessive nitrogen compounds during the combustion of the final products. Their removal by hydrodenitrogenation in multiphase reactors or possibly by liquid-phase adsorption in a packed column is, therefore, essential.

Mass transfer effects such as bulk diffusion in the pores and adsorption accompanied by surface diffusion on the pore walls of catalysts have a major influence on the efficiency of these removal processes. It is, therefore, important to establish the magnitude of the effective diffusivities and adsorption coefficients in these systems by either predictive or experimental methods. The available predictive methods for determining effective diffusivities are not adequate in systems where adsorption and surface diffusion are important and experimental methods must therefore be used. This paper describes a novel way to determine effective liquid-phase diffusivities in porous solids by measuring the transient response in a single-pellet continuous-flow system.

CONCLUSIONS AND SIGNIFICANCE

Using the developed method, the effective diffusivities of pyridine in the porous silica-alumina materials were measured to an estimated accuracy of about 20%. Advantages of the technique are: sampling is easy (even at elevated temperatures where evaporation of the liquids can cause experimental difficulties); only small amounts of fluid are required; there is no

Correspondence concerning this paper should be addressed to D. S. van Vuuren.

particle attrition; and a porous body with an ideal geometry (a plane sheet) is used.

Positive and negative changes of the measured effective diffusivities with increasing temperature were observed and explained by the contribution of surface diffusion to the net effective diffusion. Since the surface transport enhances the effective diffusivity by a factor equal to the product of the surface diffusivity and the adsorption equilibrium coefficient, temperature increases can either have a positive or a negative effect on the effective diffusivity. This is because the surface diffusivity increases and the adsorption equilibrium coefficient decreases with temperature. The surface coverage has a similar influence on the effective diffusivity when the adsorption sites are heteroenergetic because under these conditions the surface diffusivity increases and the adsorption coefficient decreases with coverage.

INTRODUCTION

Effective diffusivities of dissolved liquids in porous solids are normally determined by using stirred vessels as batch adsorbers or desorbers. The porous solids act as an adsorbent and from the rates of uptake or release of the dissolved substance the diffusivity can be calculated (Crank, 1970). Despite the usefulness of this type of arrangement, several other methods have been developed because of sampling problems, large amounts of solvents normally required, evaporation of liquids, attrition of solids, and the irregular shape of the porous particles (Kotter et al., 1975; Midoux and Charpentier, 1973; Ammons et al., 1977; Furusawa and Smith, 1974; Shibuya and Uraguchi, 1977). Since no technique is completely trouble-free, the development and evaluation of alternative methods are important.

Dynamic Wicke-Kallenbach diffusion cell arrangements have been successfully applied to determine gas-phase diffusivities (Burghardt and Smith, 1979), but are not of great value in liquid-phase studies because of the stringent pressure control which is necessary when working with liquids and because of the lengthy experimental times. By closing or removing one chamber from such a dynamic septum diffusion cell arrangement, the necessity for pressure control is avoided. In this study one chamber was removed. The arrangement can thus be classified as a single, open-chamber, dynamic Wicke-Kallenbach diffusion cell or as a plane-sheet single-pellet continuous-flow stirred tank.

EXPERIMENTAL

Materials

Four silica-alumina samples designated SA00, SA40, SA60 and SA70, containing 0, 40, 60 and 70 mass % silicon dioxide respectively, were prepared from aluminum isopropoxide and tetra-ethoxysilane following the procedure of Rouxhet et al. (1976). Pyridine dissolved in n-heptane was used as a model solution.

Adsorption Equilibria

Solutions of pyridine in n-heptane were introduced into flasks containing accurately weighed amounts of powdered silica-alumina. The well-stoppered flasks were equilibrated for more than 24 hours in a constant temperature bath while being shaken gently. After equilibration the pyridine concentration in the supernatent was measured with a Cary 219 ultraviolet spectrophotometer that had previously been calibrated. The adsorbed pyridine concentration was finally calculated using a mass balance.

Effective Diffusivities

Details of the diffusion cell assembly are shown in Figure 1. Figure 2 is a flow diagram of the system.

To prevent attrition by the stirrer the silica-alumina powder was pressed into the pellet holder so that the exposed top surface was slightly below the sample holder rim. The stirrer was a glass-covered magnetic follower driven externally by a rotating magnet.

A descending pyridine concentration step function was produced by initially circulating a pyridine in heptane solution through the cell until equilibrium was achieved. This normally took four days for the first experiment on a pellet, one day for duplicate experiments, and two days for experiments where the temperatures were changed. The flow was then changed to a pure heptane flow by a low dead volume valve.

The diffusion cell temperature was controlled by immersing the cell in a glycerine bath which was temperature controlled by a surrounding water bath. The temperature variation during a run was less than 0.5 K.

The concentration of pyridine in the effluent as a function of time was measured with a flow-through UV detector from a Perkin-Elmer LC-65T liquid chromatograph and recorded on a chart recorder.

Modelling of the Experimental Rig

A mass balance over the free cell volume gives

$$QC_i - QC - A\left(D_P \left.\frac{\partial c}{\partial x}\right|_{x=L} + \rho D_S \left.\frac{\partial c_A}{\partial x}\right|_{x=L}\right) = V\frac{dC}{dt} \qquad (1)$$

while a differential mass balance over a pellet increment gives

$$D_P \frac{\partial^2 c}{\partial x^2} + \rho D_S \frac{\partial^2 c_A}{\partial x^2} = \epsilon \frac{\partial c}{\partial t} + \rho \frac{\partial c_A}{\partial t} . \qquad (2)$$

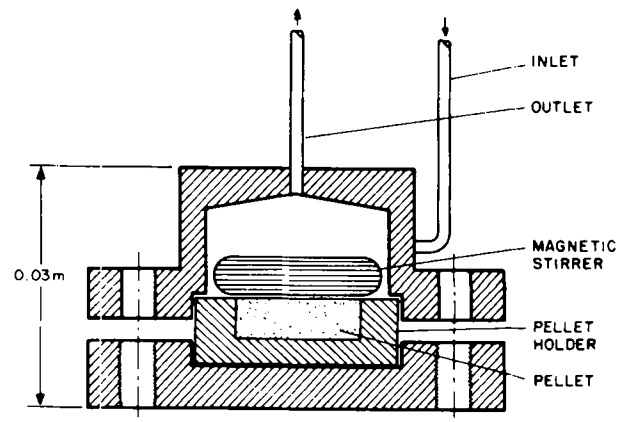

Figure 1. Details of single-pellet diffusion cell.

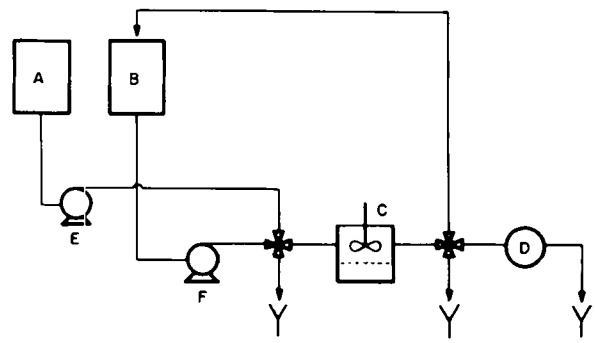

A SOLVENT RESERVOIR
B EQUILIBRATION SOLVENT RESERVOIR
C DIFFUSION CELL
D U.V. DETECTOR
E CONSTANT FLOW RATE SOLVENT PUMP
F EQUILIBRATION PUMP

Figure 2. Diffusion cell flow diagram.

TABLE 1. PELLET PROPERTIES

Catalyst	Surface Area 10^{-3} m^2/kg	Porosity	Mean Pore Radius 10^{-9} m
SA001	217	0.48	2.3
SA002	217	0.58	3.4
SA401	231	0.57	4.0
SA601	297	0.55	3.1
SA701	205	0.57	5.1

TABLE 2. FREUNDLICH PARAMETERS OF PYRIDINE ADSORPTION ISOTHERMS

Sample	Temp.	α	β
SA00	303 K	0.044	0.4854
	318 K	0.042	0.5930
	333 K	0.034	0.6801
SA40	303 K	0.046	0.2933
	318 K	0.035	0.2485
	333 K	0.034	0.2566
SA60	303 K	0.059	0.2218
	318 K	0.058	0.2521
	333 K	0.053	0.2609
SA70	303 K	0.051	0.2679
	318 K	0.046	0.2753
	333 K	0.035	0.2309

Assuming instantaneous equilibrium adsorption and a linearized adsorption isotherm (see experimentally determined adsorption isotherms) it follows that

$$c_A = K_A c + B. \tag{3}$$

Substitution of Eq. 3 in Eqs. 1 and 2 gives

$$QC_i - QC - A\,D_{EFF}\left.\frac{\partial c}{\partial x}\right|_{x=L} = V\frac{dC}{dt}$$

and

$$D_{EFF}\frac{\partial^2 c}{\partial x^2} = K_P\frac{\partial c}{\partial t}$$

where

$$D_{EFF} = D_P + \rho K_A D_S \tag{4}$$

and

$$K_P = \epsilon + \rho K_A.$$

The boundary conditions are:

$$c = C, \quad x = L$$

and

$$\frac{\partial c}{\partial x} = 0, \quad x = 0.$$

For a descending step function the initial conditions are:

$$c = C = C_0, \quad t = 0,$$

$$c_A = K_A C_0 + B, \quad t = 0,$$

and

$$C_i = 0, \quad t > 0.$$

Transforming the effluent concentration from the time domain to the Laplace domain gives

$$S(p) = \mathcal{L}[\eta(\tau)] = \int_0^\infty e^{-p\tau}\eta(\tau)\,d\tau$$

$$= \frac{1}{p} - \frac{1}{p[1 + p + \phi_2\sqrt{p}\,\tanh(\phi_1\sqrt{p})]} \tag{5}$$

where

$$\eta = C/C_0,$$

$$\tau = \frac{tV}{Q},$$

$$\phi_1 = L\sqrt{\frac{K_P Q}{D_{EFF}V}},$$

and

$$\phi_2 = A\sqrt{\frac{K_P D_{EFF}}{QV}}.$$

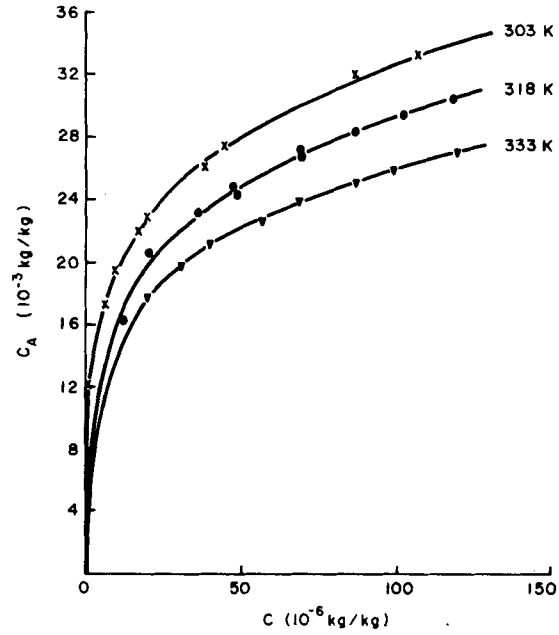

Figure 3. Adsorption on SA60.

The excessive tailing and the nonlinearity of the adsorption isotherm precluded the use of moment analysis (Ramachandran and Smith, 1978), and Eq. 5 was therefore inverted to the time domain using a numerical technique (Weeks, 1966) and the effective diffusivity evaluated by a linear Taylor differential correction least squares technique (McCalla, 1967).

A sensitivity test showed that the response is insensitive to ϕ_1 for the experimental times used in this study, the reason probably being that $\tanh(\phi_1\sqrt{p})$ tends to its asymptotic value of unity. Equation 5 can therefore be approximated by

$$S(p) \simeq \frac{1}{p} - \frac{1}{p(1 + p + \phi_2\sqrt{p})}. \tag{6}$$

Equation 6 can be inverted analytically using the complex inversion formula and integrating along a suitable Bromwich contour in the complex plane (Appendix). Three solutions exist, depending on the value of ϕ_2. Because $0 < \phi_2 < 2$ only the solution for this case is given, viz:

$$\eta(\tau) = 1 - \sqrt{\frac{\tau}{1 - (\phi_2/2)^2}}\,Im\left\{\frac{w(a + ib)}{b - ta}\right\} \tag{7}$$

where

$$a = \sqrt{\tau[1 - (\phi_2/2)^2]},$$

$$b = \frac{\sqrt{\tau}\phi_2}{2}$$

and

$$w(z) = e^{-z^2}\,\mathrm{erfc}(-iz)$$

Although it is not convenient to use Eq. 7 in computations, the equation was of value to check the accuracy of the numerical inversion technique. This was found to have an accuracy of more than three decimal digits.

RESULTS AND DISCUSSION

Pyridine was chosen as the model component because it is a common constituent of fossil-fuel liquids and has an intermediate basicity ($pK_b = 8.75$) thus preventing irreversible adsorption on highly acid silica-alumina surfaces.

Properties related to the pore structure of the experimental silica-alumina samples are given in Table 1. The specific surface areas were determined by nitrogen adsorption, and approximate porosities and mean pore radii calculated using the densities of ideal mixtures of γ-alumina and silica.

The equilibrium adsorption isotherms of pyridine on SA60 are shown in Figure 3. The shapes of the adsorption isotherms on the other samples are similar. Therefore only the parameters of the Freundlich equations ($c_A = \alpha c^\beta$) which best describe the isotherms in the "least-squares" sense are given in Table 2.

TABLE 3. DIFFUSIVITIES DETERMINED BY TIME DOMAIN FITTING

Run No.	Pellets	Porosity	Temp. K	Flow Rate 10^{-9} m^3·s^{-1}	Partition Coeff.	Diffusivity 10^{-9} m^2·s^{-1}
1	SA001	0.48	303	3.578	315	1.90
2				8.819	330	2.07
3	SA002	0.58	303	8.263	178	3.25
4				8.384	190	2.84
5			318	8.599	149	2.75
6				8.533	165	2.74
7			333	5.169	102	3.20
8	SA40	0.57	303	7.359	175	1.07
9				7.530	194	0.71
10				9.493	204	0.74
11			318	6.288	164	0.53
12				6.638	176	0.45
13			333	4.244	156	0.43
14				4.309	161	0.45
15	SA60	0.55	303	7.409	148	1.52
16				7.500	172	1.27
17			318	5.888	200	0.86
18				4.836	205	1.03
19			333	4.291	174	1.00
20				2.991	172	0.76
21	SA70	0.57	303	8.033	134	1.43
22				8.347	141	1.36
23			318	6.570	133	1.35
24				7.109	142	1.25
25			333	4.255	106	1.43
26				3.831	109	1.29

Since the experimental adsorption isotherms do not have the same form as the Langmuir isotherm at low concentrations (the Langmuir isotherm reduces to a linear isotherm at low concentrations), it follows that the adsorption sites on the silica-alumina surfaces have a distribution of energies. Sips 1950 showed that for gas adsorption on a heteroenergetic surface, the Freundlich isotherm corresponds to adsorption on a surface with a distribution of energies approaching a negative exponential function at high energies of adsorption.

To apply the equations modelling the diffusion cell system, the adsorption isotherms were linearized. Between concentrations of about 30 and 120 $\times$ 10^{-6} kg/kg linearization of the isotherms is a reasonable approximation (Figure 3). An estimate of the effect of this linearization on the experimental effective diffusivity showed that an error less than 20% results.

The diffusivities for all the runs are summarized in Table 3. All the measurements under different conditions were duplicated except in the case of the diffusivity measurement for SA60 at 333 K. The duplications show good repeatability, generally better than 20%. Since the duplications were normally done after only one day of re-equilibration, which might have been too little, more emphasis should be placed on the first measurements.

The experimental data for Run 15 and the corresponding predicted curve are given in Figure 4. The deviations of the experimental data from the predicted curves were similar in all the experiments. Since the residuals between the experimental and predicted points are not randomly distributed around the predicted curve, it follows that the probable error owing to the linear approximation of the adsorption equilibria is greater than the statistical measurement errors. These were found to give a standard

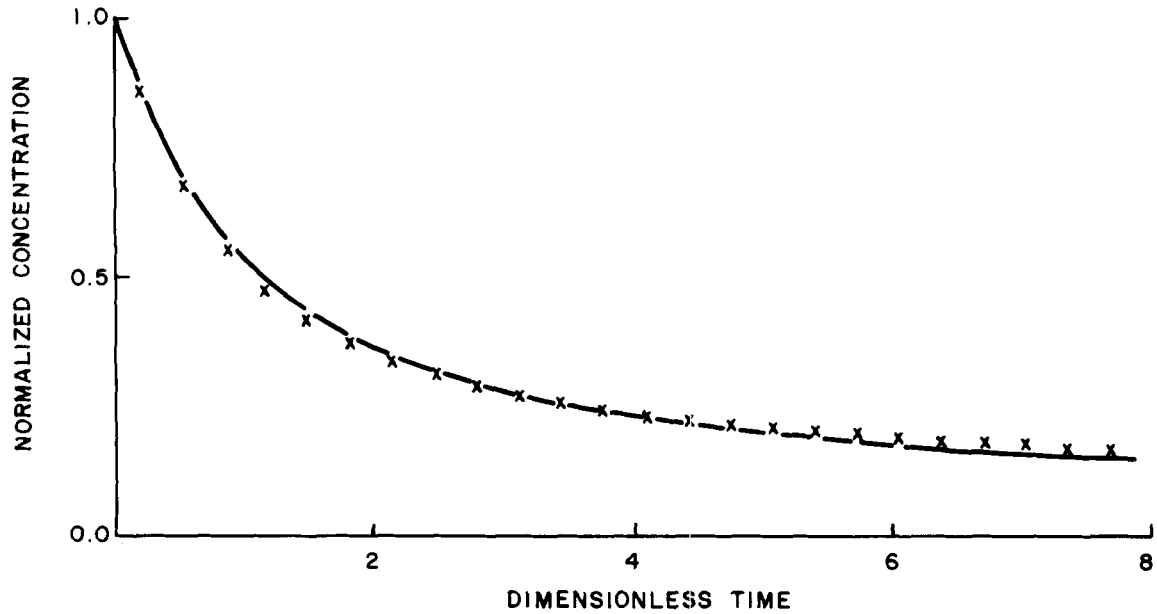

Figure 4. Experimental and predicted responses of Run 15.

TABLE 4. ESTIMATION OF SURFACE DIFFUSION COEFFICIENTS

Run No.	Catalyst	Tortuosity[1] χ	λ	Restrictivity[2] K_r	Pore Diffusivity[3] 10^{-9} m^2·s^{-1}	Surface Diffusivity 10^{-12} m^2·s^{-1}	Surface Transport / Total Transport	Surface Coverage[4] % Beginning of Run	Surface Coverage[4] % End of Run
1	SA001	4.2	0.14	0.52	0.14	5.6	0.93	6.6	3.9
3	SA002	2.5	0.097	0.64	0.44	15.8	0.86	10.3	4.2
5					0.54	14.9	0.80	7.6	2.2
7					0.63	25.4	0.80	4.9	1.3
9	SA40	2.6	0.083	0.68	0.50	1.1	0.29	16.0	8.8
11					0.61	<0	<0	13.7	8.3
13					0.71	<0	<0	12.7	7.8
15	SA60	2.8	0.11	0.61	0.40	7.6	0.74	22.2	14.9
17					0.48	2.7	0.53	18.4	12.2
19					0.56	2.5	0.44	16.6	11.3
21	SA70	2.6	0.065	0.74	0.54	6.6	0.62	24.4	14.5
23					0.67	5.1	0.50	20.6	12.9
25					0.77	6.2	0.46	16.9	12.3

[1] $\chi = \epsilon\exp[2(1/\epsilon - 1)]$ (Probst and Wohlfahrt, 1979).
[2] $K_r = 10^{-2\lambda}$ (Satterfield et al., 1973).
[3] $D_P = K_r D_{BULK}\chi/\epsilon$.
[4] Surface coverages were calculated assuming a pyridine molecule occupies 0.24×10^{-18}m^2.

deviation of 10% compared to the estimated 20% error which resulted from the approximation.

There are no data in the literature with which to compare the measured effective diffusivities given in Table 3. Since, to the author's knowledge, this is the first case where actual decreases in the effective diffusivity with increasing temperatures have been found, a comparison with existing theories is necessary to establish the validity of the results.

Equation 4 gives the dependence of the effective diffusivity on the pore and surface diffusivities. Theoretically the pore diffusivity and the surface diffusivity increase and the adsorption coefficient decreases with temperature. Depending on the magnitudes of the parameters either a decrease or an increase in the effective diffusivity can result with increasing temperature. Komiyama and Smith (1974b) proposed a theoretical model for surface diffusion. They related the surface diffusivity to the adsorption coefficient and the Gibbs free energy of activation for forming a vacant site. Depending on the magnitudes of the various parameters of their model the product of the adsorption coefficient and the surface diffusivity can either increase or decrease with temperature. The observed data do not therefore contradict their theory.

The diffusion cell response is not sensitive enough to the ratio

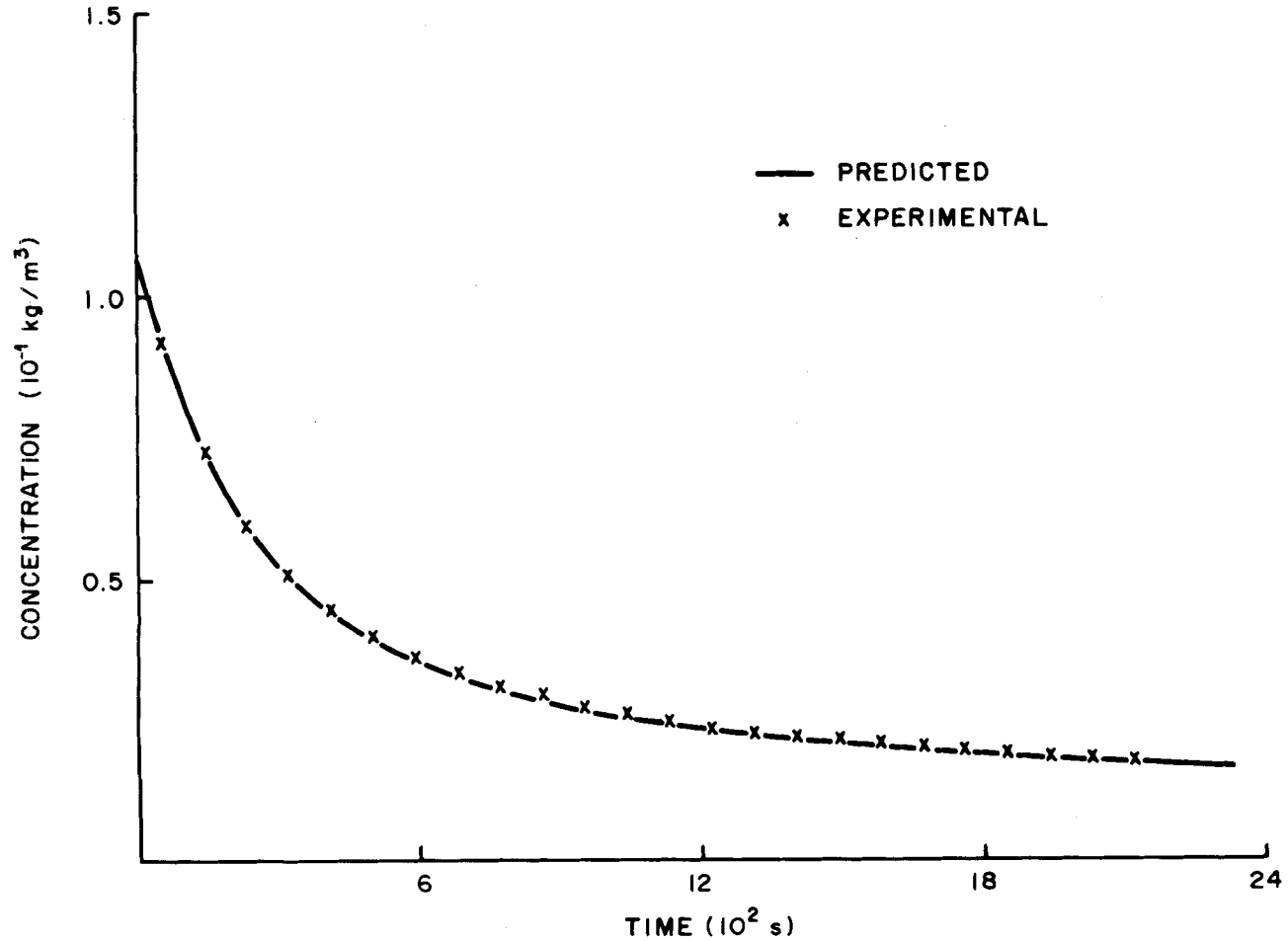

Figure 5. Finite difference numeric prediction of Run 15.

of the pore and surface diffusivities to evaluate both diffusivities from the data. To separate these effects predictive methods for the pore diffusivity can be used. The pore diffusivity is a function of the porosity, the tortuosity and the restrictivity of the pellet. Using correlations for determining tortuosities by Probst and Wohlfahrt (1979), for restrictivities by Satterfield et al. (1973) and for bulk diffusion coefficients by King et al. (Reid et al., 1977), pore diffusivities were calculated from

$$D_P = \frac{K_r D_{BULK} \chi}{\epsilon} \tag{8}$$

The surface diffusivities calculated from the experimental effective diffusivities and Eqs. 4 and 8 are given in Table 4. The decrease of some of the surface diffusivities with temperature cannot be a result of experimental error or errors in the prediction methods alone. The only other explanation is the dependence of the surface mobility on the strength of adsorption and in turn the dependence of the strength of adsorption on surface coverage.

A number of authors have shown that the surface diffusivity decreases with increasing strength of adsorption (Satterfield et al., 1973; Komiyama and Smith, 1974a,b). In this paper it has also been concluded that the adsorption sites are hetero-energetic and that the average energy of occupied sites should therefore be higher at lower surface coverages. The surface diffusivities are therefore not independent of concentration as implied by the model equations.

The diffusion runs were organized so that they had roughly the same initial pyridine concentration in the effluent. This led to lower initial and therefore lower average surface coverages for runs at higher temperatures. Lower surface diffusivities could therefore have resulted owing to this effect at higher temperatures.

A finite difference numerical solution of the model equations using the experimental Freundlich adsorption isotherm and the pore and surface diffusivities as calculated in Table 4 for Run 15 is given in Figure 5. The good agreement between the experimental and predicted curves show that the effective diffusivities as determined by the approximate linear model represent the experimental data adequately.

NOTATION

A = pellet cross-sectional area, m^2
a = dimensionless variable
B = empirical constant
b = dimensionless variable
C = concentration of solute in free cell, $kg \cdot m^{-3}$
C_i = concentration of solute in inlet stream, $kg \cdot m^{-3}$
C_0 = initial concentration of solute in free cell, $kg \cdot m^{-3}$
c = concentration of solute in pellet pores based on the pore volume, $kg \cdot m^{-3}$
c_A = concentration of solute adsorbed, based on amount adsorbed per unit mass of pellet, kg/kg
D_{BULK} = bulk liquid phase diffusivity, $m^2 \cdot s^{-1}$
D_{EFF} = effective diffusivity, $m^2 \cdot s^{-1}$
D_P = pore volume diffusivity, $m^2 \cdot s^{-1}$
D_S = surface diffusivity, $m^2 \cdot s^{-1}$
K = adsorption coefficient in Langmuir equation
K_A = equilibrium adsorption coefficient, $m^3 \cdot kg^{-1}$
K_P = partition coefficient
K_r = restrictivity
L = pellet thickness, m
p = Laplace variable
Q = volumetric flow rate, $m^3 \cdot s^{-1}$
S = Laplace transform of $\eta(\tau)$
t = time, s
V = diffusion cell volume, m^3
w = complex function, Eq. 7
x = pellet coordinate, m
z = complex variable, Eq. 7

Greek Letters

α = empirical constant in Freundlich isotherm
β = empirical constant in Freundlich isotherm
ϵ = pellet porosity
η = normalized concentration
λ = ratio of critical solute molecular diameter to pore diameter
ρ = pellet density, $kg \cdot m^{-3}$
τ = dimensionless time
ϕ_1 = dimensionless parameter, Eq. 5
ϕ_2 = dimensionless parameter, Eq. 5
χ = tortuosity

APPENDIX: ANALYTICAL INVERSION OF THE LAPLACE TRANSFORM

The Laplace transform of the response to an ascending step input function can be approximated by:

$$S(p) = \frac{1}{p(1 + p + \phi_2\sqrt{p})} \tag{A1}$$

If $\phi_2 = 2$, or if $\phi_2 > 2$, Eq. A1 can readily be reduced to forms with known inverses (Erdélyi, 1954). For the experimental conditions in this study ϕ_2 is normally less than two. The approximate inverse can be derived using the complex inversion formula:

$$\eta(\tau) = \frac{1}{2\pi i} \int_{a-i\infty}^{a+i\infty} S(p) e^{p\tau}\, dp \tag{A2}$$

Integrating along the Bromwich contour shown in Figure A1:

$$\eta(\tau) = \frac{1}{2\pi i} \lim_{R\to\infty} \left(\oint_c - \int_{BDE} - \int_{EF} - \int_{FGH} - \int_{HJ} - \int_{JKA} \right) \tag{A3}$$

Because the contour is taken on the first branch of $S(p)$, there are no poles inside the contour. Therefore

$$\oint_c S(p)\, e^{p\tau}\, dp = 0 \tag{A4}$$

$$\lim_{R\to\infty} \int_{BDE} S(p)\, e^{p\tau}\, dp = \lim_{R\to\infty} \int_{JKA} S(p)\, e^{p\tau}\, dp = 0 \tag{A5}$$

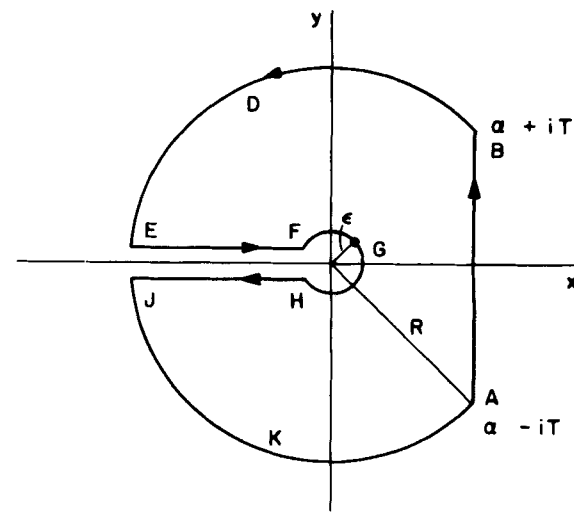

Figure A1. Bromwich contour for analytical inversion of the Laplace transform.

$$\lim_{\epsilon \to 0} \int_{FGH} S(p)\, e^{p\tau}\, dp$$

$$= \lim_{\epsilon \to 0} \int_{\pi}^{-\pi} \frac{e^{\epsilon e^{i\theta}\tau}\, i\epsilon e^{i\theta}}{\epsilon e^{i\theta}\,(1 + \epsilon e^{i\theta} + \phi_2\sqrt{\epsilon e^{i\theta/2}})}\, d\theta$$

$$= -2\pi i \tag{A6}$$

By substituting p with $ue^{i\pi} = -u$ along EF and with $ue^{-i\pi} = -u$ along HJ, the integrals along EF and HJ reduce to:

$$\lim_{\substack{R \to \infty \\ \epsilon \to 0}} \left(\int_{EF} S(p)\, e^{p\tau}\, dp + \int_{HJ} S(p)\, e^{p\tau}\, dp \right) = I$$

$$= \int_0^{\infty} \frac{2i\phi_2\sqrt{u}\, e^{-u\tau}}{u[(1-u)^2 + \phi_2^2\, u]}\, du \tag{A7}$$

Note that along EF $\sqrt{P} = i\sqrt{u}$ and along $HJ\sqrt{P} = -i\sqrt{u}$.

Substituting $u = x^2$ into Eq. A7 gives:

$$I = 4i\phi_2 \int_0^{\infty} \frac{e^{-x^2\tau}}{x^4 + (\phi_2^2 - 2)x^2 + 1}\, \mathrm{dx} \tag{A8}$$

But

$$\int_0^{\infty} \frac{2xy\, e^{-t^2}\, dt}{t^4 - 2(x^2 - y^2)t^2 + (x^2 + y^2)^2} = \frac{\pi}{2}\, Im\left(\frac{w(x + iy)}{y - ix}\right) \tag{A9}$$

(Abramowitz and Stegun, 1965).

The following substitutions reduce Eq. A8 to the same form as Eq. A9:

$$z^2 = x^2\tau \tag{A10}$$

$$a = \sqrt{\tau(1 - \phi_2^2/4)} \tag{A11}$$

$$b = \frac{\sqrt{\tau}\,\phi_2}{2} \tag{A12}$$

$$\therefore \quad I = 4i\phi_2\tau^{3/2} \int_0^{\infty} \frac{e^{-z^2}}{z^4 - 2(a^2 - b^2)z^2 + (a^2 + b^2)^2}\, dz$$

$$= \frac{i\phi_2\tau^{3/2}\pi}{ab}\, Im\left(\frac{w(a + ib)}{b - ia}\right)$$

$$= \frac{2i\pi\sqrt{\tau}}{\sqrt{1 - \phi_2^2/4}}\, Im\left(\frac{w(a + ib)}{b - ia}\right) \tag{A13}$$

where

$$w(z) = e^{-z^2}\, \mathrm{erfc}(-iz) \tag{A14}$$

LITERATURE CITED

Abramowitz, M., and I. A. Stegun, *Handbook of Mathematical Functions*, Dover Publications, New York (1965).

Ammons, R. D., N. A. Dougharty, and J. M. Smith, "Adsorption of methylmercuric chloride on activated carbon. Rate and equilibrium data," *Ind. Eng. Chem.*, **16**, 263 (1977).

Burghardt, A., and J. M. Smith, "Dynamic response of a single catalyst pellet," *Chem. Eng. Sci.*, **34**, 267 (1979).

Crank, J., *Mathematics of Diffusion*, Oxford Clarendon Press (1970).

Erdélyi, A., *Tables of Integral Transforms*, McGraw-Hill (1954).

Furusawa, T., and J. M. Smith, "Intraparticle mass transport in slurries by dynamic adsorption studies," *AIChE J.*, **20**, 88 (1974).

Komiyama, H., and J. M. Smith, "Intraparticle mass transport in liquid-filled pores," *AIChE J.*, **20**, 728 (1974a).

Komiyama, H., and J. M. Smith, "Surface diffusion in liquid-filled pores," *AIChE J.*, **20**, 1110 (1974b).

Kotter, M., P. Lovera, and L. Riekert, "Zur Bestimmung effektiver Diffusionskoeffizienten in porösen Katalysatoren," *Ber. Bunsen Gesell.*, **79**, 807 (1975).

McCalla, T. R., *Introduction to Numerical Methods in Fortran Programming*, John Wiley (1967).

Midoux, N., and J. C. Charpentier, "Apparent diffusivity and tortuosity in a liquid-filled porous catalyst used for hydrodesulfurization of petroleum products," *Chem. Eng. Sci.*, **28**, 2108 (1973).

Probst, K., and K. Wohlfahrt, "Empirische Abschätzung effektiver Diffusionskoeffizienten in porösen Systemen," *Chem. Ing. Tech.*, **51**, 737 (1979).

Ramachandran, P. A., and J. M. Smith, "Transport rates by moment analysis of dynamic data," *Ind. Eng. Chem. Fund.*, **17**, 148 (1978).

Reid, R. C., J. M. Prausnitz, and T. K. Sherwood, *The Properties of Gases and Liquids*, 3rd Ed., McGraw-Hill (1977).

Rouxhet, P. G., et al., "The chemistry and surface chemistry of oxides in the silica-alumina range," *Coll. Interface. Sci.*, **V**, 81 (1976).

Satterfield, C. N., C. K. Colton, and W. H. Pitcher, Jr., "Restricted diffusion in liquids within fine pores," *AIChE J.*, **19**, 628 (1973).

Shibuya, H., and Y. Uraguchi, "Effective diffusivities in activated carbon pellets by a dynamic Wicke-Kallenbach apparatus," *J. Chem. Eng. Japan*, **10**, 446 (1977).

Sips, R., "On the structure of a catalyst surface II," *J. Chem. Phys.*, **18**, 1024 (1950).

Weeks, W. T., "Numerical inversion of Laplace transforms using Laguerre functions," *J. Ass. Comp. Mach.*, **13**, 419 (1966).

Manuscript received November 18, 1982; revision received June 22, and accepted July 1, 1983.